Controlled synthesis of NaYF 4 :Yb,Er upconversion nanocrystals as potential probe for bioimaging: A focus on heat treatment

Alireza Kavand, Christophe A Serra, Christian Blanck, Marc Lenertz, Nicolas Anton, Thierry F Vandamme, Yves Mély, Frédéric Przybilla, Delphine Chan-Seng

Controlled synthesis of $NaYF_4$:Yb,Er upconversion nanocrystals as potential probe for bioimaging: A focus on heat treatment

Alireza Kavand,[1,2] Christophe A. Serra,[1,] Christian Blanck,[1] Marc Lenertz,[3] Nicolas Anton,[2] Thierry F. Vandamme,[2] Yves Mély,[4] Frédéric Przybilla,[4] Delphine Chan-Seng[1]*

[1] Université de Strasbourg, CNRS, Institut Charles Sadron UPR 22, Strasbourg, F-67000, France

[2] INSERM (French National Institute of Health and Medical Research), UMR 1260, Regenerative Nanomedicine (RNM), FMTS, Université de Strasbourg, Strasbourg, F-67000, France

[3] Université de Strasbourg, CNRS, IPCMS UMR 7504, Strasbourg, F-67000, France

[4] Université de Strasbourg, CNRS, Laboratoire de Bioimagerie et Pathologies UMR 7021, Strasbourg, F-67000, France

* corresponding author : serrac@ecpm.u-strasbg.fr

ABSTRACT

Upconversion nanoparticles are a promising class of materials for bioimaging. Their attractive optical properties are influenced by their crystalline phase, size, and morphology resulting from the preparation method employed. Herein, we synthesized $NaYF_4$:Yb,Er nanocrystals by the co-precipitation method followed by a heat treatment step. The influence of the treatment temperature and the type of reactor on the phase transition from the α-cubic to the β-hexagonal phase was investigated. We found that before the phase transition, the size and shape of α-$NaYF_4$:Yb,Er nanocrystals evolved due to a coalescence mechanism with microtubular reactors. In contrast to the flask system, we also observed an anisotropic growth of β-$NaYF_4$:Yb,Er nanorods in microtubes whose length can be controlled by adjusting the temperature. The diameter of microtubes plays a critical role in the shape evolution of the final products from spheres to nanorods. The type of reactor and thus the resulting temperature gradient could be considered as a promising parameter to control the phase, shape and size of UCNPs without changing the chemical composition.

KEYWORDS: Upconversion nanoparticles, $NaYF_4$ nanocrystals, nanorods, spherical particle, phase transition, size control, flask, microtube

1. INTRODUCTION

Through the last decade, lanthanide-doped upconversion nanoparticles (UCNPs) have been widely investigated for their potential applications in a large range of areas, such as therapeutics, multimodal bioimaging, solar cells, sensors, high-density optical storage, deep ultraviolet lasing, photolithography and three-dimensional flat-panel displays.[1–7] Numerous investigations have been reported on rare-earth (RE) doped fluorides UCNPs especially $NaYF_4$ nanocrystals because of their excellent properties such as low phonon energy (< 400 cm^{-1}) and excellent chemical stability.[8,9] Several methods for producing these nanocrystals have been developed, which include co-precipitation, thermal decomposition, hydrothermal synthesis, sol-gel synthesis, combustion synthesis, and flame synthesis.[8] The synthesis of $NaREF_4$ nanocrystals by the co-precipitation method comprises two steps that include first the precipitation at low temperature followed by a post-treatment at high temperature (typically around 300 °C).[10]

These nanocrystals have two major types of crystalline structures, cubic α-phase and hexagonal β-phase, the latter exhibiting higher luminescence intensity.[11] Cubic α-phase with lower forming energy is the first to be produced during the synthesis that is later converted into β-phase following a treatment at high temperature. Many investigations on the phase transition to control of nanocrystals' size, shape and luminescence intensity report, for example, the introduction of trivalent lanthanide dopant ions with larger radius, such as Gd^{3+},[12] the doping with alkali ions (Li^+ or K^+ ions),[13] the use of mixtures of surfactants such as oleic acid, oleylamine, and tributylphosphine,[14–16] the effect of the chemicals concentration ratio (oleic acid, octadecene, NaOH, and NH_4F),[17–20] the replacement of sodium oleate by oleic acid,[21] the addition of separated or combined solutions of NH_4F and NaOH,[22] the effect of the reaction time and temperature.[23,24] Significant efforts have also been invested in the characterization of their growth and phase transition mechanism.[25–32] Suter *et al.* have investigated the growth of nanocrystals and the transition from cubic α-phase to hexagonal β-phase in real-time by monitoring their NIR-to-visible upconversion emission.[30] They have defined four stages related to the evolution of $NaYF_4$ nanocrystals during the heat treatment step, in which the longest period of time is between the initial formation of the small cubic α-phase nanocrystals and the start of the phase transition that was called relative stasis phase. May *et al.* have studied the

mechanism of crystals growth by a mathematical model,[32] while Radunz *et al.* have investigated the evolution of size and optical properties of $NaYF_4$ nanocrystals with different techniques such as small-angle X-ray scattering (SAXS), transmission electron microscopy (TEM), X-ray powder diffraction (XRD) and inductively coupled plasma atomic emission spectroscopy (ICP-OES).[26]

To the best of our knowledge, despite significant efforts invested in controlling the phase, shape, and growth of nanocrystals, no study has been focused on the effect of the type of vessels used and their inherent heat transfer rates on the growth of $NaLnF_4$ nanocrystals. In this study, the selection of an appropriate reactor for the growth of $NaYF_4$:Yb,Er nanocrystals during the heat treatment step was considered. We designed a system for the heat treatment step based on stainless steel microtubes that can be used at different lengths with capacities ranging from several milliliters to a few hundred milliliters affording an easy access to scale-up. In addition to the advantage of scale-up, these tubes as closed systems, allow eliminating some of the parameters that have a tangible effect on the final product such as argon gas flow, stirring rate, and volume of the mixture for reaction.[33] The simultaneous control of all these parameters is frequently difficult and nanocrystals may differ from batch to batch. This can be avoided by using microtubes that allow the control of these parameters and thus improve the repeatability of the growth process of nanocrystals.

2. EXPERIMENTAL SECTION

2.1. Materials

Yttrium(III) chloride hexahydrate (99.99%), ytterbium(III) chloride hexahydrate (99.99%), erbium(III) chloride hexahydrate (99.99%), oleic acid (technical grade, 90%), 1-octadecene (technical grade, 90%), sodium hydroxide (anhydrous, ACS reagent, ≥97%), and ammonium fluoride (ACS reagent, ≥98.0%) were purchased from Sigma-Aldrich. Ethanol (absolute, 99.99%). Cyclohexane (99.8%), methanol (99.8%), and acetone (99.8%) were purchased from Carlo Erba.

2.2 Synthesis of $NaYF_4$:Yb^{3+},Er^{3+} nanocrystals

$NaYF_4$:20% Yb^{3+}, 2% Er^{3+} nanocrystals were synthesized according to a previously reported procedure in two steps with some modifications (Scheme 1).[10]

Formation of primary nuclei. Yttrium(III) chloride hexahydrate (0.78 mmol, 237 mg), ytterbium(III) chloride hexahydrate (0.2 mmol, 78 mg), and erbium (III) chloride hexahydrate (0.02 mmol, 8 mg)

were added into a solution of oleic acid (6 mL) and 1-octadecene (15 mL) in a 50 mL three-neck round bottom flask. The mixture was heated to 150 °C under an argon atmosphere and vigorous stirring. Once a homogeneous solution was obtained, it was cooled to 30 °C. A mixture of NaOH (2.5 mmol, 0.100 g) and NH_4F (4 mmol, 0.145 g) in 5 mL of methanol was added dropwise to the solution and stirred for 30 min at 30 °C. To remove methanol, the temperature was increased stepwise (15 min at 80 °C and then 15 min at 110 °C) and finally the reactive medium was placed under vacuum for 10 min at 110 °C to remove the last traces of methanol and moisture.

Heat treatment in flask systems. The mixture was heated to a given temperature (290, 300, 305, or 310 °C) for 30, 60, 90, 120, or 180 min under an argon atmosphere.

Heat treatment in microtubes. The primary solution was transferred to a 20 mL syringe under argon atmosphere and then injected in the microtube with a fixed internal diameter (ID of 4083, 1753, or 876 µm) previously filled with argon by applying three cycles of argon-vacuum. Microtube' inlet and outlet were then sealed (no flow through) and the tubular reactor was thus operated as a batch reactor with no stirring. The microtubes were placed into a thermoregulated oven at a fixed temperature (290, 300, 305, 310, or 315 °C) and maintained at this temperature for different times (30 to 330 min) and then cooled to room temperature.

Product recovery. The products were precipitated by adding acetone, collected by centrifugation, and redispersed into cyclohexane.

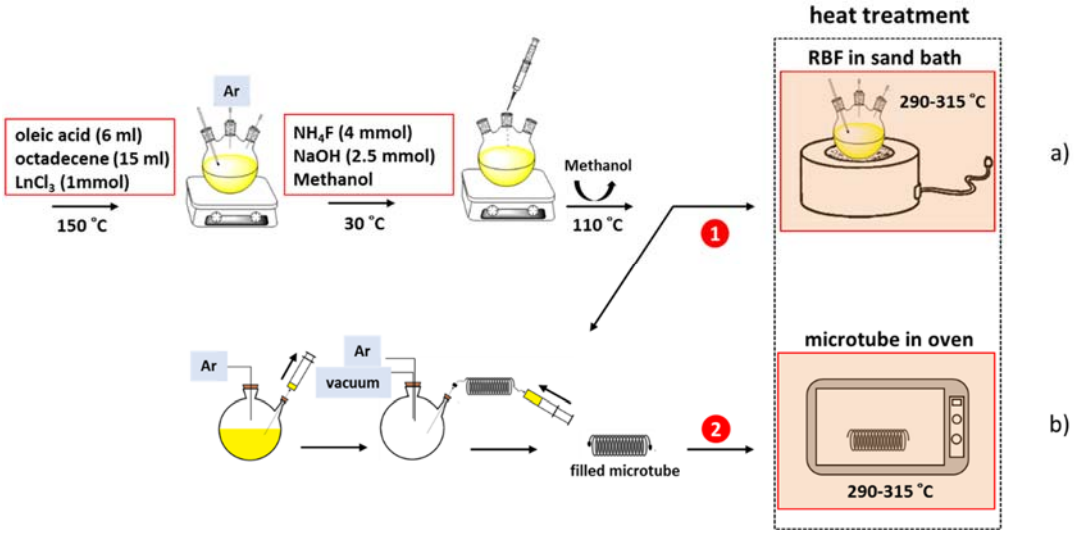

Scheme 1. General approach for the synthesis of $NaYF_4$:Yb,Er nanocrystals in a round bottom flask (RBF, a) and in a microtubular reactor along with the representation of the method employed for filling it with the primary solution (b).

2.3 Characterizations of nanocrystals

High-resolution transmission electron microscopy (HRTEM) images were obtained using a Tecnai G2 microscope (FEI) at 200 kV. 5 µL of the nanocrystals suspension in cyclohexane was deposited onto a carbon-covered copper grid (400 mesh). The suspension was left for 15 seconds and excess remove using a filter paper. Images were acquired with an Eagle2K ssCCD camera (FEI). The size distributions of the samples based on HRTEM images for more than 100 particles were investigated by the open-source ImageJ software (Version 1.51n, Wayne Rasband, National Institutes of Health, USA). The primary investigation about size evolution of nanocrystals was conducted by dynamic light scattering (DLS) (Malvern Zetasizer nano series) in cyclohexane. The helium-neon laser (4 mW) was operated at 633 nm, the scatter angle was fixed at 173° and the measurements were performed in triplicates at 25 °C. The XRD measurements were carried out on a Bruker D8 Advance powder diffractometer in the Bragg-Brentano geometry. The diffractometer was equipped with a front monochromator (Cu Kα1 wavelength λ = 0.154 056 nm) and a LynxEye linear detector. Some of the diffraction patterns were refined by profile matching method (Lebail refinement) with an anisotropic crystal shape model using Fullprof software.[34]. This allows to relate the crystal shape with its orientation. Luminescence spectra of UCNPs were obtained using a homemade setup as described in details in our previous work.[35] Briefly, the excitation at 980 nm was provided by a continuous-wave laser coupled to a single mode fiber with a maximum output of 350 mW (Qphotonics, QFBGLD-980-350), whereas the emission was collected on a fiber-optic spectrometer (Avantes, AvaSpec-3648).

3. RESULTS AND DISCUSSION

3.1 Comparison of nanocrystals growth and phase transition in a microtube and a round-bottom flask

One of the most common protocol for the synthesis of $NaYF_4$:Ln^{3+} nanocrystals by the co-precipitation method consists in mixing a 1.0 mmol of rare-earth chloride, 4.0 mmol NH_4F, 2.5 mmol NaOH, 6 mL of oleic acid and 15 mL of octadecene before applying, a heat treatment at 300 to 310 °C.[10] Using this typical formulation, we investigated the influence of the geometry of the reactor on the heat treatment step by following the growth of the nanocrystals and by determining their crystal structure.

As a reference, we selected the most widely used round-bottom flask reactor (RBF) and we applied a 300 °C heat treatment. As shown in Figure 1a, the size of the nanocrystals increased with the heat treatment time before reaching a plateau value. A careful HRTEM investigation of the samples obtained after different heat treatment times revealed that β nucleation was already observed after 30 min. Indeed, as seen on Figure 1b, two populations of nanocrystals coexisted, small α-phase crystals and larger β-phase crystals. After 120 min, phase transition was completed since HRTEM micrograph revealed only the presence of bigger nanocrystals with an interplanar spacing of 0.52 nm corresponding to the (1010) plane of β-$NaYF_4$:Yb,Er (Figure 1c).

The influence of the reactor on the growth of crystals and phase control was investigated using microtubes with various internal diameters (879, 1753, and 4083 μm that will be referred later as $microtube_{879}$, $microtube_{1753}$, and $microtube_{4083}$ respectively) as alternate heating systems. The volume of each microtube was kept constant and equal to 5.3 mL by adjusting their length to 900, 220 and 40 cm respectively. The filled microtubes were placed in an oven equipped with a sensitive thermometer. The oven set temperature was considered as the temperature of the reaction media. Indeed, given the high surface to volume ratio of the microtubes and their small inner diameters, it is assumed that the temperature gradient from their external surface to their center is small. We started with $microtube_{4083}$ at 300 °C with different heat treatment times and compared it to the RBF (Figure 1a). In contrast to the RBF, experiments conducted in $microtube_{4083}$ showed that the nucleation process of the β-phase was delayed by approximately 120 min. Indeed, HRTEM images revealed that only cubic α-phase nanocrystals were present after 120 min heating since the observed lattice fringe with a spacing of ~0.31 nm correspond to the (111) d-spacing of α-$NaYF_4$:Yb,Er (Figure 1d). This observation was confirmed by an XRD analysis (Figure S1). However, when the heat treatment time was increased to 180 min, β nucleation clearly occurred since bigger particles coexisted with smaller α-phase nanocrystals (Figure 1e). The (α→ β) phase transition continued over time so that after 330 min heat treatment no α-phase nanocrystal could be observed anymore (Figure 1f) in agreement with the completion of the nanocrystal growth phase. Interestingly, whereas the RBF reactor produced nearly solely spherical β-$NaYF_4$:Yb,Er nanocrystals with an average diameter of 30.1 ± 0.7 nm, the microtubular reactor produced β-$NaYF_4$:Yb,Er nanorods with a length of 48 ± 12 nm and a width of 22 ± 2 nm

(Figure 1f). The influence of the type of reactor and temperature on the β-phase transition time range and the shape of nanocrystals will be discussed in depth in Sections 3.2 and 3.3 respectively.

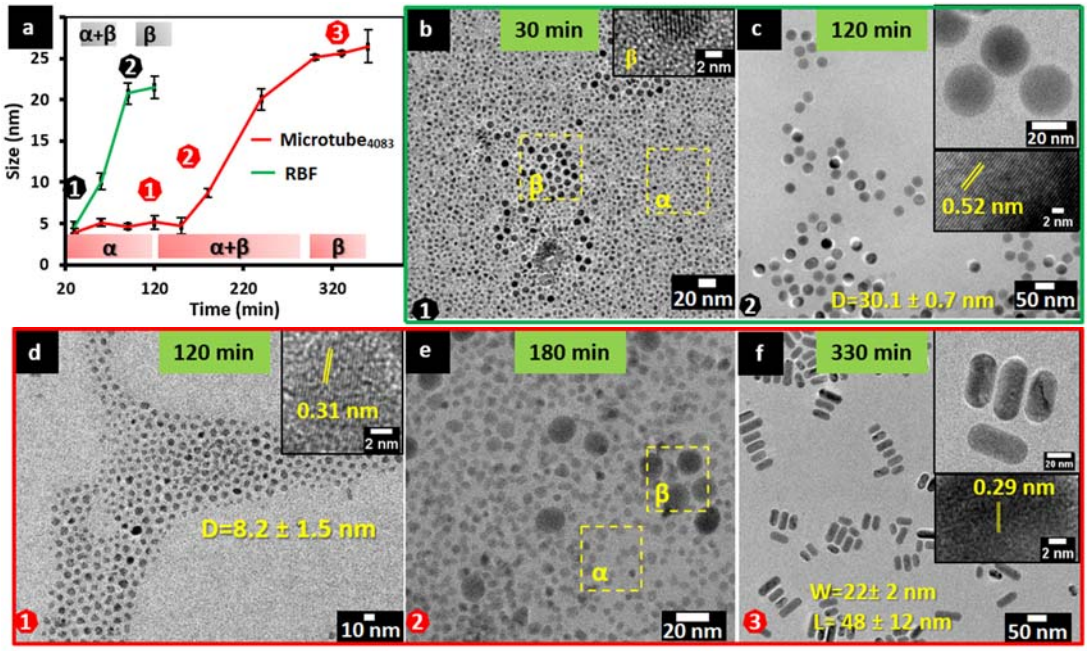

Figure 1. Evolution of the size of the nanocrystals (determined by DLS) during the heat treatment step at 300 °C for RBF and microtube$_{4083}$ (a). HRTEM images of nanocrystals synthesized at 300 °C in the flask (b and c) and microtube (d-f) systems: mixture of cubic and hexagonal phase (RBF, 30 min) (b), hexagonal β-phase nanocrystals (RBF, 120 min) (c), cubic phase (microtube$_{4083}$, 120 min) (d), mixture of cubic and hexagonal β-phase (microtube$_{4083}$, 180 min) (e), and hexagonal β-phase (microtube$_{4083}$, 330 min) (f). Insets show images of nanocrystals at higher magnifications and the lattice fringes.

3.2 Influence of temperature and type of reactor on the time range of β-phase transition

The experiments conducted in the microtube system showed that the dissolution process of the cubic α-phase nanocrystals (α→ β) proceeded with a slow rate, despite the high heat transfer and subsequent temperature homogeneity of the microtube compared to the flask system (see Section 3.2.4). From the previous results, it seems that the low rate of dissolution of cubic α-phase nanocrystals in microtube led to a low concentration of monomers for β-phase nucleation (*i.e.* below supersaturation for crystallization). Ultrasmall β-phase nuclei are thermodynamically less stable than α-phase nuclei.[36] Therefore, at a low concentration of monomers, β-phase nuclei after being formed do not have the opportunity to reach the critical radius corresponding to the

minimum size that allow them to survive in solution without being redissolved (and thus evolving back to α-phase[22,37]). In contrast, if the concentration of monomers is high enough in the system (*i.e.* supersaturation), the β-phase nuclei can reach the critical size above which they can survive.[17,38] In conclusion, the type of reactor seems to have a strong effect on the time scale over which a heat treatment had to be applied for the phase transition to occur. In order to confirm this assumption, experiments with smaller ID were performed.

3.2.1 Comparison of nanocrystals growth in large and small ID microtubes (4083 and 879 µm)

We used a microtube with an internal diameter (ID) of 879 µm, which is about 4.5-fold smaller than the previous one, microtube$_{4083}$. The morphologies and crystal-phase of the resultant $NaYF_4$:Yb,Er nanocrystals at various heating times were investigated by HRTEM and XRD (Figure 2 and Figure S2). The images showed that β-phase nucleation occurred already after 60 min of heating and resulted in a mixture of α-phase nanocrystals having an average size of 5.7 ± 1.2 nm and β-phase nanocrystals with a narrow size distribution (9.4 ± 0.6 nm) as shown in Figure 2c. Increasing the heating time led to an overall increase of the size of β-phase nanocrystals with a broadening of their size distribution as well as a change in their morphology from spherical to rod-like shape (Figure 2d). The resultant β-$NaYF_4$:Yb,Er nanocrystals for 150 min of heating (Figure 2f) included a mixture of spherical (13 ± 2 nm) and rod-like (23 ± 4 nm in length) β-phase nanocrystals. One could also observe residual α-phase nanocrystals.

Two major differences can be identified by comparing microtube$_{879}$ and microtube$_{4083}$, namely the β-phase nucleation time range and the size distribution of the nanocrystals. The first β-phase nanocrystals were observed after 60 min of heating in microtube$_{879}$ whereas 180 min of heating was needed for microtube$_{4083}$. On the other hand, the β-phase nanocrystals from microtube$_{879}$ had a poor size distribution compared to the larger ID microtube. The consumption of cubic α-phase nanocrystals, β-phase nucleation, and growth of β-phase nanocrystals overlapped strongly in the smaller microtube. For this reactor, after 150 min of heating, spherical β-$NaYF_4$:Yb,Er nanocrystals with a diameter ranging from 10 nm to 18 nm coexisted with 40 nm long axis nanorods (Figure 2f). For the larger microtube (4083 µm), the new nucleation (from the smallest β-phase nanocrystals, <10 nm) apparently stopped at 180 min heating time favoring the growth

of more uniform crystals as supported by the presence of monodisperse spherical β-phase nanocrystals (~18 nm, Figure 1e).

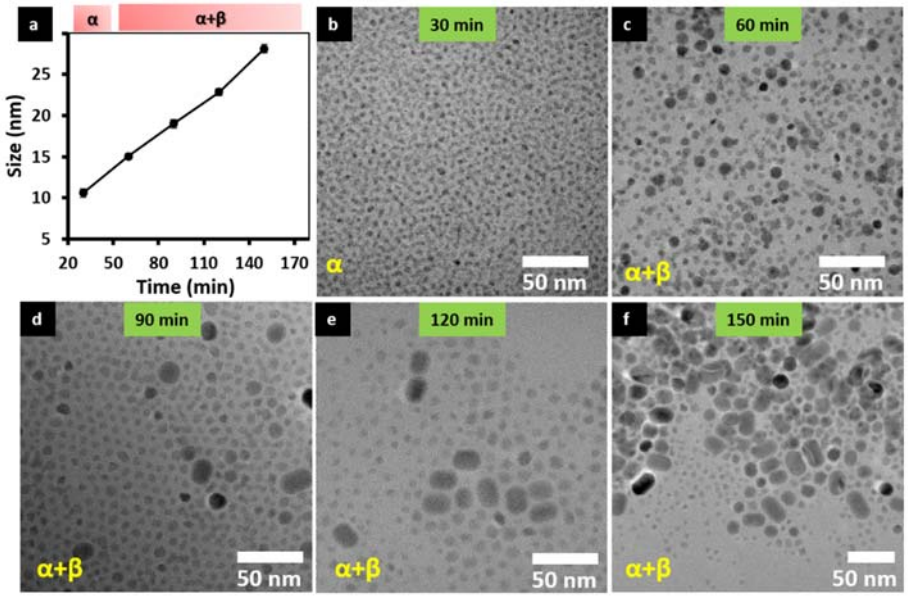

Figure 2. Size evolution (determined by DLS) (a) and HRTEM images of $NaYF_4$:Yb,Er nanocrystals obtained in microtube$_{879}$ (b-f), heated at 300 °C after different heating times.

3.2.2 Growth of nanocrystals into microtube$_{879}$ at higher temperature (310 °C) for various heat treatment times

At this stage, one can question the effect of temperature and the possibility of getting narrow size distribution of β-phase nanocrystals in the smaller microtube. In order to further investigate the effect of the temperature on the formation of $NaYF_4$:Yb,Er nanocrystals, the experiment was repeated in microtube$_{879}$ at 310 °C. The nanocrystals obtained after 30 min of heating had a cubic α-phase as reported by XRD analysis (Figure S3), in agreement with HRTEM images that indicated lattice fringes of 0.31 nm characteristic of α-$NaYF_4$:Yb,Er nanocrystals (Figure 3a). These spherical nanocrystals were highly monodisperse with a diameter of 5.9 ± 0.5 nm. After 60 min of heating, a bimodal distribution of α-phase nanocrystals was observed, where small and spherical nanocrystals coexisted with bigger nanocrystals having an irregular shape (Figure 3b). Increasing the heat treatment to 90 min led to an increase in the particle size up to 8.3 ± 1.8 nm (Figure 3b-c) without altering their crystalline phase as indicated by HRTEM (see inset in Figure 3a-c) and confirmed by XRD (Figure S3). At 90 min, the majority of the α-$NaYF_4$:Yb,Er nanocrystals had an irregular shape with a broad size distribution (Figure 3c). The XRD results indicated the presence

of single α-phase nanocrystals without any impurity (Figure S3) in agreement with the ~0.31 nm lattice fringes in the HRTEM images (Figure 3c).

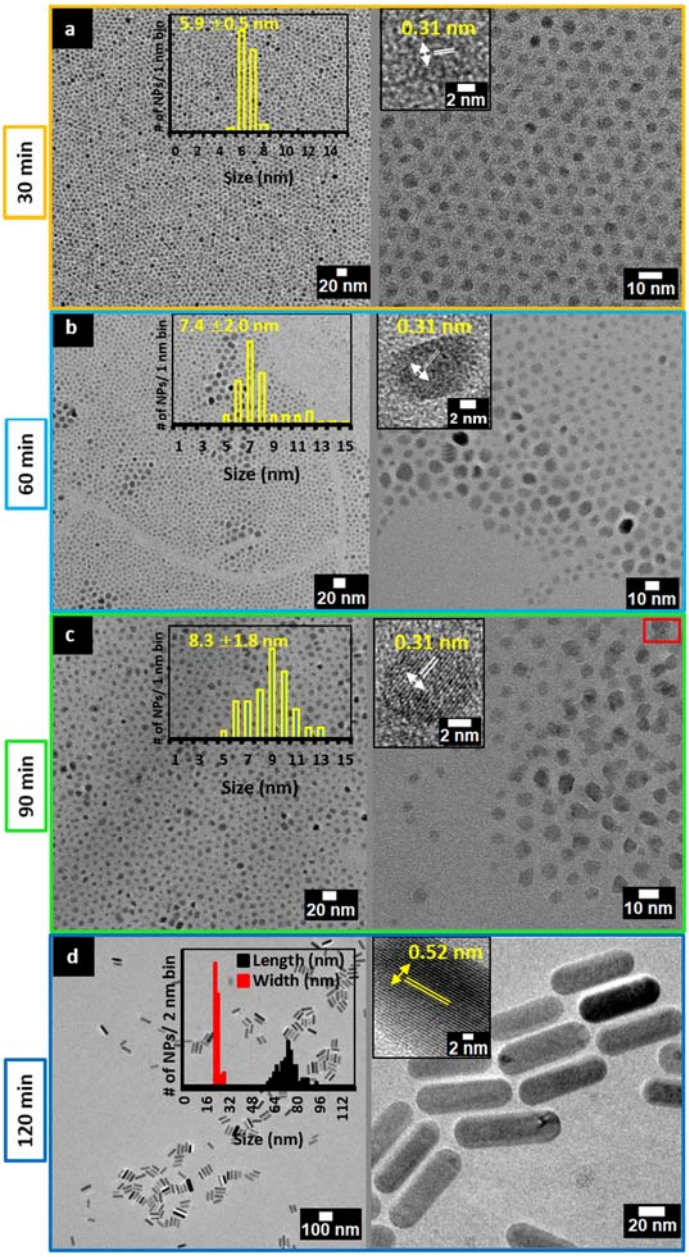

Figure 3. HRTEM images at two magnifications of $NaYF_4$:Yb,Er nanocrystals synthesized at 310 °C in microtube$_{879}$ after different heating times, 30 (a), 60 (b), 90 (c) and 120 min (d). The red box on the micrograph at 90 min highlights a zoom reported in Figure 4.

The upconversion emission of the α-$NaYF_4$:Yb,Er nanocrystals obtained after 30 and 90 min of heating was measured under the same conditions and concentrations in cyclohexane (40 mg·mL^{-1}) (Figure S4). The α-$NaYF_4$:Yb,Er nanocrystals obtained after 90 min of heating showed a

twofold increase in intensity compared to the nanocrystals obtained after 30 min of heating. This increase may result from a lower amount of crystal defects induced by the rearrangement of atoms in the internal and surface structure of nanocrystals as well as the growth in nanocrystal size during the heating process and thus a more favorable surface to volume ratio. A meticulous investigation of the HRTEM micrographs of the irregular α-$NaYF_4$:Yb,Er nanocrystals obtained after 90 min of heating revealed several occurrences of sintering between two nanocrystals (Figure 4). The resulting sintered nanocrystals are then tougher to relax into a spherical nanocrystal larger than the two initial nanocrystals (Figure 4), which supports an oriented attachment mechanism, *i.e.* coalescence process[39] during the nanocrystal growth phase.

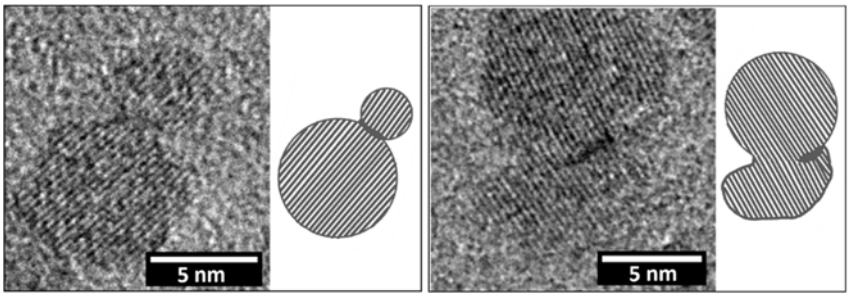

Figure 4. Two examples of sintering of α-$NaYF_4$:Yb,Er nanocrystals by coalescence mechanism in microtube$_{879}$ at 310 °C after 90 min of heating.

Therefore, it seems that the primary step for phase transition (α→ β) could be the growth of small α-phase nanocrystals followed by a coalescence process which led to larger nanocrystals. The coalescence process could be driven by surface energy reduction because the surface area of a newly formed nanocrystal was less than that of the sum of the surface areas of the primary nanocrystals. Overall, our results are in agreement with the work of Lee *et al.*[40] who showed that oriented attachment is an effective mechanism for the formation of anisotropic nanocrystals under hydrothermal annealing. Their results, such as the change in the morphology of primary nanocrystals from spherical to anisotropic and production irregular-shaped nanocrystal by heat treatment, are consistent with our results.

An induction period before the phase transition towards β-phase nanocrystals is commonly observed for $NaYF_4$ nanocrystals. According to Suter *et al.*, the heating time before phase transition (>25 min) could be defined as a relative stasis of α-phase nanocrystals population.[30] However, this mechanism is still unclear. Our results strongly suggested that the α-phase

nanocrystals may also grow by the coalescence process beside the Ostwald ripening phenomenon that was reported in the literature.[26,30,32]

Surprisingly, despite the high temperature (310 °C) and homogeneous heat transfer of the microtube$_{879}$, one could not observe any hexagonal β-phase with HRTEM before 90 min of heating. This was probably related to the slow change in shape and size of the α-phase nanocrystals.

As shown in Figure 3d after 120 min of heating, all nanocrystals had a rod-like shape with narrow size distribution. Their average size was 73 ± 6 nm in length and 22 ± 1 nm in width (Figure 3d). Obtaining β-$NaYF_4$:Yb,Er nanocrystals was confirmed by HRTEM image displaying an interplanar spacing of 0.52 nm (Figure 3d) and by XRD analysis (Figure S5). The hexagonal crystal system of the β-phase with rod-like shaped nanoparticles suggests a preferential growth along the [00l] direction. This was investigated by refining the XRD pattern with an anisotropic shape model (Fig S5b) leading to a mean shape of the crystallites of 72 nm along [00l] and around 16 nm along the [hk0] directions. This is in agreement with the TEM images and confirms the preferential grow along the [001] axis. A sharp phase transition occurred between 90 min and 120 min during the heat treatment step, since all the α-phase nanocrystals were converted into the β-phase nanocrystals. Na *et al.* have prepared β-$NaYF_4$:Yb,Er nanorods (L = 60.1 nm and W = 21.5 nm) with the same components but with a higher ratio of oleic acid to solvent (9.5 *vs.* 0.4 in the present study) and slightly higher temperature (*i.e.* 320 °C *vs.* 310 °C) in a flask system.[20] In order to check the repeatability of our microtube system for nanorod synthesis, the 150 min heating experiment was duplicated. The resultant β-$NaYF_4$:Yb,Er nanoparticles had a size (L = 76 ± 7 nm and W = 22 ± 1 nm) comparable to those produced in the initial experiments, indicating that the system has a good repeatability for the formation of nanorods (Figure S6).

In summary, the growth of nanocrystals in microtube$_{879}$ at 310 °C included two steps: i) growth and subsequent accumulation of irregularly shaped α-phase nanocrystals and ii) fast phase transition (α→ β) which produced pure β-$NaYF_4$:Yb,Er nanorods. For the first stage, it seems that irregularly shaped α-$NaYF_4$:Yb,Er nanocrystals could be the mature-form of the cubic α-phase. This type of nanocrystal could be less stable than primary cubic nanocrystals despite their larger size. This instability may be due to different interactions of the oleic acid (capping agent) on the

surface of the nanocrystals (*i.e.* strong coordination interaction or weak Van der Waals interaction) as explained by Mai *et al.* for α-$NaYF_4$:Yb,Er nanocrystals with different shapes and sizes. If the adhesion energy or interaction on the surface is low, the chances of instability and dissolution of the nanocrystal will be high.[27] On the other hand, nanocrystals with irregular or anisotropic shapes have lower stability compared to spherical nanocrystals of the same volume due to their higher surface areas which renders them metastable.[27,41] Therefore, dissolution of this type of nanocrystals should be a source of monomers for the growth of β-phase nanocrystals. As observed in microtubular reactors the phase transition happened when most of the cubic α-phase spherical nanocrystals became irregular in shape with a critical size around 12 nm. It seems that as the number of this type of metastable nanocrystal in the system went up, *e.g.* when heating time was increased, more monomers were produced by their dissolution. As a result, the concentration of monomers reached a critical concentration thus initiating the second stage: β nucleation (Figure 5).

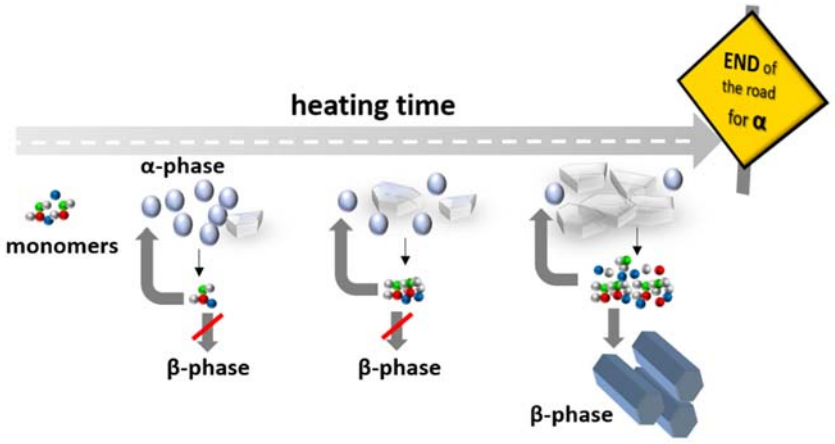

Figure 5. Schematic illustration of size, morphology and phase evolution of $NaYF_4$:Yb,Er nanocrystals when increasing the heating time from 30 to 120 min at 310 °C in $microtube_{879}$.

3.2.3 Size and morphology of α-phase nanocrystals before full conversion in β-phase nanocrystals at different temperatures for the flask system

To get a deeper insight, we studied the size and morphology of α-$NaYF_4$:Yb,Er nanocrystals before full conversion of the cubic α-phase into hexagonal β-phase for the flask system at 310 °C. In contrast to $microtube_{879}$, after 30 min of heating, a mixture of cubic and hexagonal phase was observed. The HRTEM images showed that the size and morphology of α-$NaYF_4$:Yb,Er nanocrystals were similar to those of nanocrystals produced with the microtube before phase

transition (Figure S7a). An additional 30 min heating time led to a complete dissolution of the α-$NaYF_4$:Yb,Er nanocrystals and production of pure β-$NaYF_4$:Yb,Er (Figure S7b). The formation of these irregular α-$NaYF_4$:Yb,Er nanocrystals was also investigated at 290 °C in the flask system. As seen in Figure S8 both size and shape were similar to the α-$NaYF_4$:Yb,Er nanocrystals observed at 310 °C and obtained either with the flask or the microtubular reactor.

Overall, if one compares the time for nucleation and growth of β-phase in flasks and microtubes at 310 °C, it can be concluded that the β nucleation happened faster in flasks. This may be interpreted by considering that a homogeneous heat transfer system (microtube) could impede the formation of irregular α-$NaYF_4$:Yb,Er nanocrystals by suppressing the coalescence process. Therefore, the accumulation of these nanocrystals as a source of monomers for β-phase transition could be delayed. An additional reason may be the high pressure inside the microtube which may slow down the dissolution of irregular α-$NaYF_4$:Yb,Er nanocrystals. The collision between two nanocrystals is another critical parameter for promoting the coalescence process.[40,42] It is also worth to note that the microtubes were devoid of any physical source of mixing. To summarize, our experiments suggested that a system with heterogeneous heat transfer facilitated phase transition (α→ β).

3.2.4 Comparison of nanocrystals growth in different temperature gradient reactors

In order to get a better insight on the underlying mechanism, we used two different stirred flask systems (Erlenmeyer flask (EF) and RBF) at 290 °C that present different heat transfers (Figure S9). The EF presents the highest temperature gradient (~100 °C) between its flat bottom in contact with the hot plate (temperature higher than 390 °C) and the bulk of the liquid at 290 °C (set temperature); while the RBF exhibits a temperature gradient three times lower (30 °C) between its external wall (320 °C) and its center (290 °C).

The phase transition of the cubic to hexagonal phase (α→ β) in these two systems was studied by HRTEM at different heating times. We found that the consumption of α-$NaYF_4$:Yb,Er nanocrystals and phase transition in EF took approximately 120 min to reach a pure β-phase; whereas it took approximatively 180 min for the RBF. As shown in Figure 6a and b, after 150 min of heating in the RBF a mixture of α- and β-phases was observed while for the EF only β-$NaYF_4$:Yb,Er could be observed (XRD analyses in Figure 6c). The particle size of hexagonal

β-phase after full conversion of cubic α-phase in the EF was 27.6 ± 0.5 nm and in the RBF 26.6 ± 0.6 nm. The difference in the consumption rate of the cubic α-phase (120 min compared to 180 min of heating for EF and RBF, respectively) confirmed that high temperature gradients could facilitate the phase transition, in line with our previous assumption.

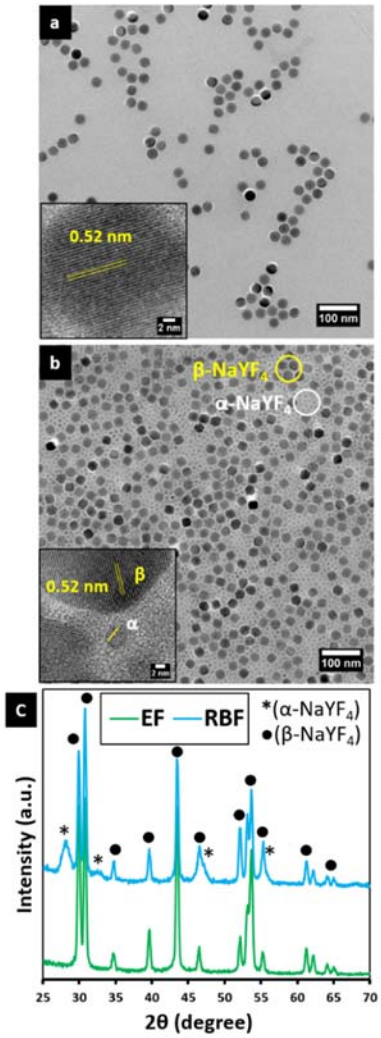

Figure 6. HRTEM images of $NaYF_4$ nanocrystals obtained using the EF (a), the RBF (b) and XRD analyses of the resulting nanocrystals after 150 min of heating at 290 °C (c).

In addition, we observed that the (α→β) phase transition did not happen in microtube$_{879}$ at 290 °C after 150 min (HRTEM in Figure S10), a system considered to have a small temperature gradient owing to its high surface to volume ratio. Therefore, the temperature gradient appeared as an important parameter for the phase transition.

As reported by Yin and Alivisatos,[41] nanocrystal growth depends upon the capability of the surfactant for on/off-exchange at the crystal surface. This exchange of surfactant is strongly affected by the temperature and occurs rapidly at higher temperatures. Since the temperature gradient for the EF is significantly higher than for the round-bottom one, the α-phase nanocrystals near its inner wall are exposed to a higher temperature. As a result, aggregation and dissolution of α-phase nanocrystals could more likely occur due to the fast exchange of surfactant molecules.

3.3 Influence of temperature, heating time and type of reactor on the shape of β-phase nanocrystals

From the first set of experiments (Section 3.1 and Figure 1), it was observed that the shape of the β-phase nanocrystals was different when the crystals were produced with a RBF or a microtubular reactor. In the following, we will focus on the different parameters affecting the shape and size of the β-phase nanocrystals.

3.3.1 Nanocrystals produced in microtubes with different internal diameters and at different temperatures

In a new set of experiments, the synthesis of β-$NaYF_4$:Yb,Er nanocrystals was carried out at different temperatures from 300 to 315 °C with microtubes of different internal diameters (4083 and 1753 μm). HRTEM images and size distribution histograms of β-$NaYF_4$:Yb,Er nanocrystals are presented in Figure S11, Figure S12 and Figure S13. As shown in Figure S11, the β-$NaYF_4$:Yb,Er nanocrystals synthesized in $microtube_{4083}$ at 305 °C after 180 min of heating were shorter in length than those obtained with $microtube_{1753}$. However, it is noteworthy to mention that the widths of these nanocrystals had roughly the same value. At 310 °C the size (length and width) and size distribution of β-$NaYF_4$:Yb,Er nanocrystals were significantly different for both microtubes (Figure S12). The nanorods prepared at 315 °C with both microtubes had the same length (*ca.* 39 nm) and width (*ca.* 21 ± 3 nm) (Figure S13a and b). However, the nanocrystals from $microtube_{4083}$ had uniform shape and narrow size distribution compared to $microtube_{1753}$.

All information about the lengths and widths of the as-synthesized nanorods is summarized in Figure 7. Overall, the results obtained with the two microtubes showed that β-$NaYF_4$:Yb,Er nanocrystals grown in the longitudinal direction. On the other hand, the transversal growth of

nanocrystals was less influenced by the temperature and the diameter of the microtube. Consequently, the width of the nanorods remained at the same value of *ca*. 20-22 nm.

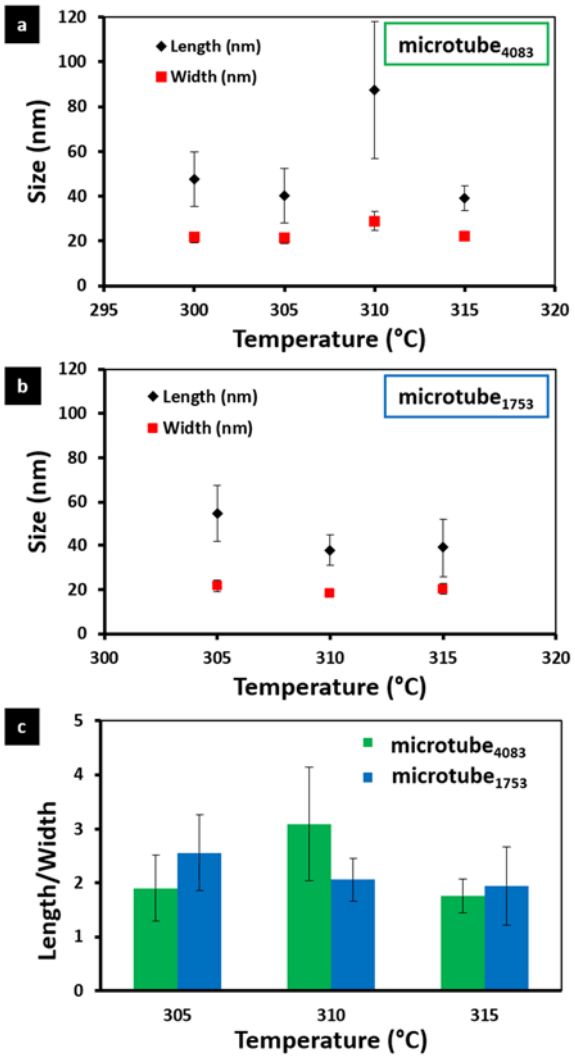

Figure 7. Length and width evolution of β-$NaYF_4$:Yb,Er nanorods as a function of the temperature and internal diameter of microtube: 4083 µm (a), 1753 µm (b). Length/width ratio of nanorods in the two microtubes at different temperatures (c).

3.3.2 Step by step study of β-phase nanocrystals growth

By monitoring the growth processes of nanocrystals in $microtube_{4083}$ for different reaction times but constant temperature (310 °C), it was observed that the nanocrystals had a growth in the longitudinal direction at an almost constant width (Figure 8a). The size of the β-phase nanocrystals increased by a symmetric growth once a spherical nanocrystal of 18 nm was formed after a set point of 90 min of heating. The β-phase nanocrystals evolved then from a spherical

shape to nanorods by increasing their length. Moreover, the temperature seemed to affect this set point. For example, the longitudinal growth of the β-phase nanocrystals for the same microtube heated at 300 °C started after about 180 min of heating (Figure S14) while at 315 °C it was after 60 min (Figure S15). The average size of nanocrystal increased stepwise until all the cubic α-phase was consumed. Based on these results, it seems that the new nucleation of β-phase stopped and β-phase nanocrystals had an asymmetric growth in the longitudinal direction. Anisotropic shapes such as nanorods are formed when nucleation is stopped, which can occur at low concentration of monomer.[43] However, in flask, the concentration in monomer was higher due to the fast dissolution of α nanocrystals affording spherical shapes after full consumption of the cubic α-phase (Figure 8b). Before the full conversion of cubic α-phase, β-phase nanocrystals had a hexagonal shape that evolved into a spherical shape presumably due to symmetric growth.

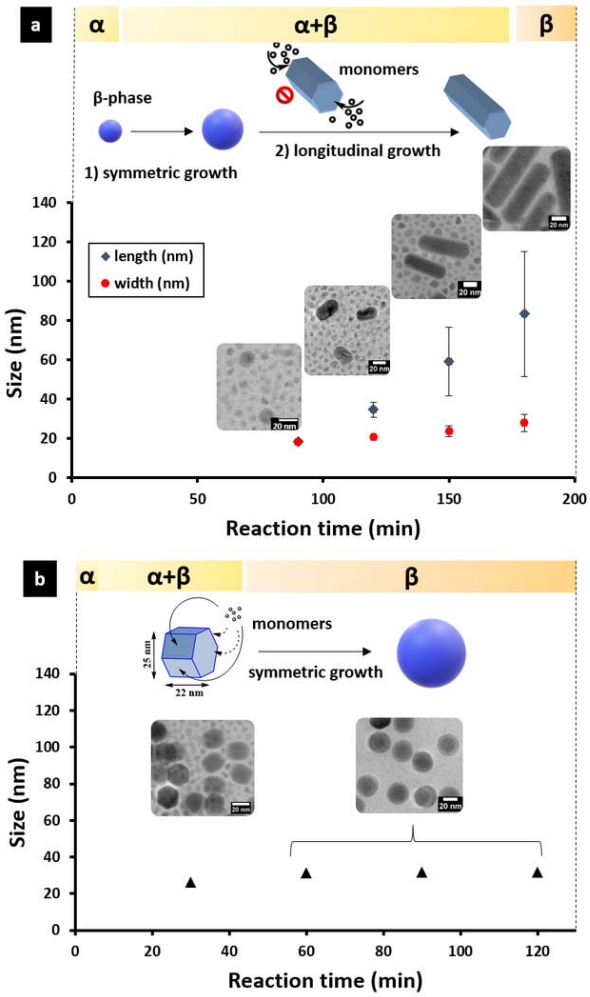

Figure 8. Longitudinal growth of β nanocrystals at 310 °C in microtube$_{4083}$ (a) and symmetric growth of β nanocrystals in RBF (b) at different times. Insets are the corresponding β-$NaYF_4$:Yb,Er nanocrystals HRTEM images.

3.3.3 Summary of nanocrystal phase evolution at different temperatures, heating times and reactors

In order to precisely represent the influence of the temperature, heat treatment time and type of heating system on nanocrystals phase, three graphs were plotted. The complete phase transition point and details related to the type of phase for different conditions are reported in Figure 9. The size evolution, phase, and shapes of nanocrystals were extracted from HRTEM images and DLS measurements (Figure S16). From these data, we can conclude that microtube$_{4083}$ and microtube$_{1753}$ almost had the same phase transition pattern than the flask system. The main difference was that the phase transition in these microtubes was much slower.

The nanocrystals produced in microtube$_{879}$ at 290 °C were only cubic α-phase while at 300 °C, a mixture of α- and β-phases was observed. Interestingly, a sharp phase transition was observed in microtube$_{879}$ at 310 °C, which was not observed for other conditions. Furthermore, increasing the temperature led to increasing phase transition rate. In fact, high temperature facilitates the formation of hexagonal phase by increasing dissolution of cubic phase.

The upconversion luminescence of all β-$NaYF_4$:Yb,Er nanocrystals was validated by spectroscopy measurements gathered in Figure S17.

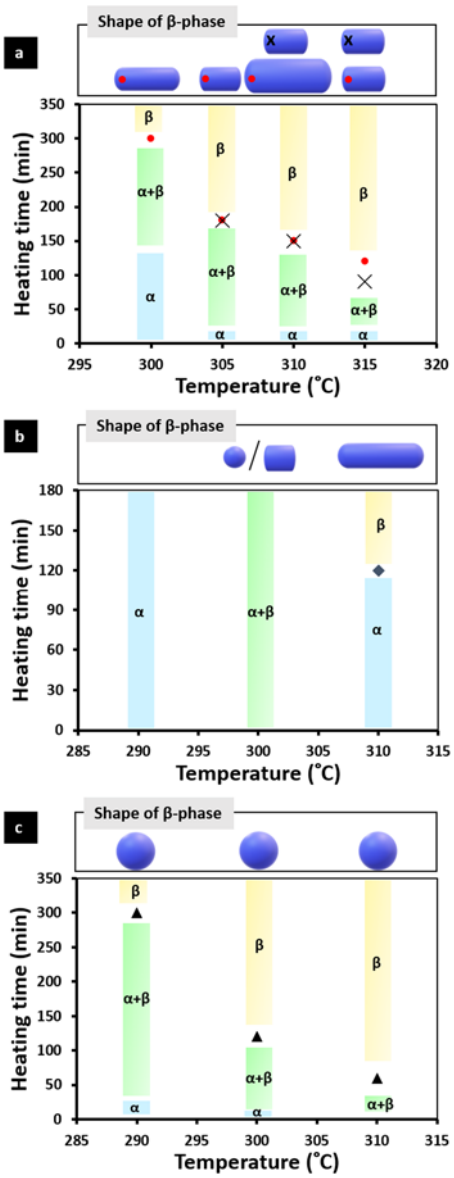

Figure 9. Summary information on the phase evolution of $NaYF_4$:Yb,Er nanocrystals as a function of temperature and heating time for $microtube_{4083}$ (circle) and $microtube_{1753}$ (cross) (a), $microtube_{879}$ (b) and RBF system (c). Circle, cross, diamond and triangle represent the time points at which the pure phase β-$NaYF_4$:Yb,Er nanocrystals are formed.

4. CONCLUSION

The size, crystalline phase and shape of $NaYF_4$:Yb,Er nanocrystals, synthesized by the co-precipitation method followed by a heat treatment at high temperature (above 300 °C), proved to be highly dependent on the type of reactor used for the heat treatment. At a given temperature, the phase transition between the α-cubic and β-hexagonal phases was much faster for reactors characterized by high temperature gradients, like the Erlenmeyer flask, as compared

to low temperature gradient reactors such as the round-bottom flask or microtubes. Given the slow growth of β-$NaYF_4$:Yb,Er nanocrystals in microtubes, we could detect two populations of nanocrystals with cubic α-phase before phase transition. We thus observed for the very first time that α-$NaYF_4$:Yb,Er nanocrystals passed through an anisotropic metastable intermediate by a coalescence mechanism, similar to the so-called oriented attachment, before to rearrange and dissolve to give rise to the β-$NaYF_4$:Yb,Er nanocrystals by Ostwald ripening. Delay in phase transition for the microtubes could also be attributed to the building pressure inside, low collision possibility of nanocrystals and homogeneous heating which hindered the coalescence. We also found that in the microtubular reactors, the β-$NaYF_4$:Yb,Er nanocrystals grew in an anisotropic hexagonal shape (nanorods) conversely to the flask systems for which only spherical nanocrystals were produced. The length of the nanorods could be changed with heating temperature while the width remained relatively constant. In perspective, microtubes could be considered for β-$NaYF_4$:Yb,Er nanocrystals production scale-up when operating in continuous-flow and used to investigate the phase transition of other formulations. Continuous-flow production is recognized to provide a high degree of reproducibility over time. Large batch reactors are known to exhibit chemicals' concentration and temperature gradients due to inhomogeneous mixing which will likely induce the coexistence of α and β nanocrystals. Thus, the use of microtube appear as an asset for the production and control of β-$NaYF_4$:Yb,Er nanocrystals as potential probe for bioimaging.

ASSOCIATED CONTENT

Supporting Information. The Supporting Information is available free of charge on the ACS Publications website at DOI:10.1021/xx. Additional data on XRD analyses, luminescence spectra, HRTEM images and size measurement by DLS at different temperatures and using different microtubes.

Author Contributions. The manuscript was written through contributions of all authors. All authors have given approval to the final version of the manuscript.

Notes. The authors declare no competing financial interest.

ACKNOWLEDGMENTS

The electronic microscopy and polymer characterization platforms at the ICS and the XR platform at the IPCMS are acknowledged for the use of their instruments. The authors are grateful to P. Petit for using some equipment related to the production of nanocrystals in microtubes and A. Collard for technical support.

REFERENCES

(1) Zhou, B.; Shi, B.; Jin, D.; Liu, X. Controlling Upconversion Nanocrystals for Emerging Applications. *Nat. Nanotechnol.* **2015**, *10* (11), 924–936.

(2) Li, Y.; Zhao, L.; Xiao, M.; Huang, Y.; Dong, B.; Xu, Z.; Wan, L.; Li, W.; Wang, S. Synergic Effects of Upconversion Nanoparticles $NaYbF_4$:Ho^{3+} and ZrO_2 Enhanced the Efficiency in Hole-onductor-free Perovskite Solar Cells. *Nanoscale* **2018**, *10* (46), 22003–22011.

(3) Chen, G.; Qiu, H.; Prasad, P. N.; Chen, X. Upconversion Nanoparticles: Design, Nanochemistry, and Applications in Theranostics. *Chem. Rev.* **2014**, *114* (10), 5161–5214.

(4) González-Béjar, M.; Francés-Soriano, L.; Pérez-Prieto, J. Upconversion Nanoparticles for Bioimaging and Regenerative Medicine. *Front. Bioeng. Biotechnol.* **2016**, *4*, 47.

(5) Zhang, Z.; Shikha, S.; Liu, J.; Zhang, J.; Mei, Q.; Zhang, Y. Upconversion Nanoprobes: Recent Advances in Sensing Applications. *Anal. Chem.* **2019**, *91* (1), 548–568.

(6) Chen, X.; Jin, L.; Kong, W.; Sun, T.; Zhang, W.; Liu, X.; Fan, J.; Yu, S. F.; Wang, F. Confining Energy Migration in Upconversion Nanoparticles towards Deep Ultraviolet Lasing. *Nat. Commun.* **2016**, *7* (1), 1–6.

(7) Sun, T.; Li, Y.; Ho, W. L.; Zhu, Q.; Chen, X.; Jin, L.; Zhu, H.; Huang, B.; Lin, J.; Little, B. E.; Chu, S. T.; Wang, F. Integrating Temporal and Spatial Control of Electronic Transitions for Bright Multiphoton Upconversion. *Nat. Commun.* **2019**, *10* (1), 1–7.

(8) Kumar, D.; Verma, K.; Verma, S.; Chaudhary, B.; Som, S.; Sharma, V.; Kumar, V.; Swart, H. C. Recent Advances in Enhanced Luminescence Upconversion of Lanthanide-doped $NaYF_4$ Phosphors. *Phys. B Condens. Matter* **2018**, *535*, 278–286.

(9) Renero-Lecuna, C.; Martín-Rodríguez, R.; Valiente, R.; González, J.; Rodríguez, F.; Krämer, K. W.; Güdel, H. U. Origin of the High Upconversion Green Luminescence Efficiency in β-$NaYF_4$:2%Er^{3+},20%Yb^{3+}. *Chem. Mater.* **2011**, *23* (15), 3442–3448.

(10) Li, Z.; Zhang, Y. An Efficient and User-friendly Method for the Synthesis of Hexagonal-phase

$NaYF_4$:Yb, Er/Tm Nanocrystals with Controllable Shape and Upconversion Fluorescence. *Nanotechnology* **2008**, *19* (34), 345606.

(11) Shi, F.; Wang, J.; Zhai, X.; Zhao, D.; Qin, W. Facile Synthesis of β-$NaLuF_4$: Yb/Tm Hexagonal Nanoplates with Intense Ultraviolet Upconversion Luminescence. *CrystEngComm* **2011**, *13* (11), 3782–3787.

(12) Wang, F.; Han, Y.; Lim, C. S.; Lu, Y.; Wang, J.; Xu, J.; Chen, H.; Zhang, C.; Hong, M.; Liu, X. Simultaneous Phase and Size Control of Upconversion Nanocrystals through Lanthanide Doping. *Nature* **2010**, *463* (7284), 1061–1065.

(13) Mao, C.; Yang, X.; Zhao, L. Simultaneous Morphology Control and Upconversion Fluorescence Enhancement of $NaYF_4$:Yb,Er Crystals through Alkali Ions Doping. *Chem. Eng. J.* **2013**, *229*, 429–435.

(14) Liu, Q.; Sun, Y.; Yang, T.; Feng, W.; Li, C.; Li, F. Sub-10 nm Hexagonal Lanthanide-doped $NaLuF_4$ Upconversion Nanocrystals for Sensitive Bioimaging in Vivo. *J. Am. Chem. Soc.* **2011**, *133* (43), 17122–17125.

(15) Ostrowski, A. D.; Chan, E. M.; Gargas, D. J.; Katz, E. M.; Han, G.; Schuck, P. J.; Milliron, D. J.; Cohen, B. E. Controlled Synthesis and Single-particle Imaging of Bright, sub-10 nm Lanthanide-doped Upconverting nanocrystals. *ACS Nano* **2012**, *6* (3), 2686–2692.

(16) Shan, J.; Ju, Y. Controlled Synthesis of Lanthanide-doped $NaYF_4$ Upconversion Nanocrystals via Ligand Induced Crystal Phase Transition and Silica Coating. *Appl. Phys. Lett.* **2007**, *91* (12), 123103.

(17) Shan, J.; Ju, Y. A Single-step Synthesis and the Kinetic Mechanism for Monodisperse and Hexagonal-phase $NaYF_4$:Yb, Er Upconversion Nanophosphors. *Nanotechnology* **2009**, *20* (27), 275603.

(18) Liu, D.; Xu, X.; Du, Y.; Qin, X.; Zhang, Y.; Ma, C.; Wen, S.; Ren, W.; Goldys, E. M.; Piper, J. A.; Dou, S.; Liu, X.; Jin, D. Three-dimensional Controlled Growth of Monodisperse sub-50 nm Heterogeneous Nanocrystals. *Nat. Commun.* **2016**, *7*, 10254.

(19) Liu, X.; Zhang, X.; Tian, G.; Yin, W.; Yan, L.; Ruan, L.; Yang, Z.; Xiao, D.; Gu, Z. A Simple and Efficient Synthetic Route for Preparation of $NaYF_4$ Upconversion Nanoparticles by Thermo-decomposition of Rare-earth Oleates. *CrystEngComm* **2014**, *16* (25), 5650–5661.

(20) Na, H.; Woo, K.; Lim, K.; Jang, H. S. Rational Morphology Control of β-$NaYF_4$:Yb,Er/Tm

Upconversion Nanophosphors Using a Ligand, an Additive, and Lanthanide Doping. *Nanoscale* **2013**, *5* (10), 4242–4251.

(21) Ye, S.; Xiao, P.; Liao, H.; Li, S.; Wang, D. Fast Synthesis of Sub-10 nm β-$NaYF_4$:Yb^{3+}, Er^{3+}@$NaYF_4$ Core-shell Upconversion Nanocrystals Mediated by Oleate Ligands. *Mater. Res. Bull.* **2018**, *103*, 279–284.

(22) Zhai, X.; Wang, Y.; Liu, X.; Liu, S.; Lei, P.; Yao, S.; Song, S.; Zhou, L.; Feng, J.; Zhang, H. A Simple Strategy for the Controlled Synthesis of Ultrasmall Hexagonal-phase $NaYF_4$:Yb,Er Upconversion Nanocrystals. *ChemPhotoChem* **2017**, *1* (8), 369–375.

(23) Zhang, C.; Lee, J. Y. Prevalence of Anisotropic Shell Growth in Rare Earth Core–shell Upconversion Nanocrystals. *ACS Nano* **2013**, *7* (5), 4393–4402.

(24) Johnson, N. J. J.; van Veggel, F. C. J. M. Sodium Lanthanide Fluoride Core-shell Nanocrystals: A General Perspective on Epitaxial Shell Growth. *Nano Res.* **2013**, *6* (8), 547–561.

(25) Liang, X.; Wang, X.; Zhuang, J.; Peng, Q.; Li, Y. Synthesis of $NaYF_4$ Nanocrystals with Predictable Phase and Shape. *Adv. Funct. Mater.* **2007**, *17* (15), 2757–2765.

(26) Radunz, S.; Schavkan, A.; Wahl, S.; Würth, C.; Tschiche, H. R.; Krumrey, M.; Resch-Genger, U. Evolution of Size and Optical Properties of Upconverting Nanoparticles During High-temperature Synthesis. *J. Phys. Chem. C* **2018**, *122* (50), 28958–28967.

(27) Mai, H. X.; Zhang, Y. W.; Sun, L. D.; Yan, C. H. Size- and Phase-controlled Synthesis of Monodisperse $NaYF_4$:Yb,Er Nanocrystals from a Unique Delayed Nucleation Pathway Monitored with Upconversion Spectroscopy. *J. Phys. Chem. C* **2007**, *111* (37), 13730–13739.

(28) Komban, R.; Klare, J. P.; Voss, B.; Nordmann, J.; Steinhoff, H.-J.; Haase, M. An Electron Paramagnetic Resonance Spectroscopic Investigation on the Growth Mechanism of $NaYF_4$:Gd Nanocrystals. *Angew. Chem. Int. Ed.* **2012**, *51* (26), 6506–6510.

(29) Voß, B.; Nordmann, J.; Uhl, A.; Komban, R.; Haase, M. Effect of the Crystal Structure of Small Precursor Particles on the Growth of β-$NaREF_4$ (RE = Sm, Eu, Gd, Tb) Nanocrystals. *Nanoscale* **2013**, *5* (2), 806–812.

(30) Suter, J. D.; Pekas, N. J.; Berry, M. T.; May, P. S. Real-time-monitoring of the Synthesis of β-$NaYF_4$:17% Yb,3% Er Nanocrystals using NIR-to-Visible Upconversion Luminescence. *J. Phys. Chem. C* **2014**, *118* (24), 13238–13247.

(31) Rinkel, T.; Nordmann, J.; Raj, A. N.; Haase, M. Ostwald-ripening and Particle Size Focussing

of sub-10 nm $NaYF_4$ Upconversion Nanocrystals. *Nanoscale* **2014**, *6* (23), 14523–14530.

(32) May, P. B.; Suter, J. D.; May, P. S.; Berry, M. T. The Dynamics of Nanoparticle Growth and Phase Change During Synthesis of β-$NaYF_4$. *J. Phys. Chem. C* **2016**, *120* (17), 9482–9489.

(33) Palo, E.; Tuomisto, M.; Hyppänen, I.; Swart, H. C.; Hölsä, J.; Soukka, T.; Lastusaari, M. Highly Uniform Up-converting Nanoparticles: Why You Should Control Your Synthesis Even More. *J. Lumin.* **2017**, *185*, 125–131.

(34) Rodríguez-Carvajal, J. Recent Advances in Magnetic Structure Determination by Neutron Powder Diffraction. *Phys. B Phys. Condens. Matter* **1993**, *192* (1–2), 55–69.

(35) Dukhno, O.; Przybilla, F.; Muhr, V.; Buchner, M.; Hirsch, T.; Mély, Y. Time-dependent Luminescence Loss for Individual Upconversion Nanoparticles upon Dilution in Aqueous Solution. *Nanoscale* **2018**, *10* (34), 15904–15910.

(36) Ayyub, P.; Palkar, V. R.; Chattopadhyay, S.; Multani, M. Effect of Crystal Size Reduction on Lattice Symmetry and Cooperative Properties. *Phys. Rev. B* **1995**, *51* (9), 6135–6138.

(37) Thanh, N. T. K.; Maclean, N.; Mahiddine, S. Mechanisms of Nucleation and Growth of Nanoparticles in Solution. *Chem. Rev.* **2014**, *114* (15), 7610–7630.

(38) Mai, H.-X.; Zhang, Y.-W.; Si, R.; Yan, Z.-G.; Sun, L.; You, L.-P.; Yan, C.-H. High-quality Sodium Rare-earth Fluoride Nanocrystals: Controlled Synthesis and Optical Properties. *J. Am. Chem. Soc.* **2006**, *128* (19), 6426–6436.

(39) Zhang, J.; Huang, F.; Lin, Z. Progress of Nanocrystalline Growth Kinetics Based on Oriented Attachment. *Nanoscale* **2010**, *2* (1), 18–34.

(40) Lee, E. J. H.; Ribeiro, C.; Longo, E.; Leite, E. R. Oriented attachment: An Affective Mechanism in the Formation of Anisotropic Nanocrystals. *J. Phys. Chem. B* **2005**, *109* (44), 20842–20846.

(41) Yin, Y.; Alivisatos, A. P. Colloidal Nanocrystal Synthesis and the Organic–inorganic Interface. *Nature* **2005**, *437* (7059), 664–670.

(42) Xue, X.; Penn, R. L.; Leite, E. R.; Huang, F.; Lin, Z. Crystal Growth by Oriented Attachment: Kinetic Models and Control Factors. *CrystEngComm* **2014**, *16* (8), 1419–1429.

(43) Liz-Marzán, L. M.; Grzelczak, M. Growing Anisotropic Crystals at the Nanoscale. *Science* **2017**, *356* (6343), 1120–1121.